Chemical Science

ROYAL SOCIETY OF CHEMISTRY

EDGE ARTICLE

View Article Online
View Journal | View Issue

Cite this: *Chem. Sci.*, 2020, **11**, 4631

All publication charges for this article have been paid for by the Royal Society of Chemistry

Solvent effects leading to a variety of different 2D structures in the self-assembly of a crystalline-coil block copolymer with an amphiphilic corona-forming block†

Shaofei Song, [a] Qing Yu, [a] Hang Zhou, [a] Garion Hicks, [a] Hu Zhu, [a] Chandresh Kumar Rastogi, [a] Ian Manners [b] and Mitchell A. Winnik *[ac]

We describe a polyferrocenyldimethylsilane (PFS) block copolymer (BCP), PFS_{27}-*b*-P($TDMA_{65}$-*ran*-$OEGMA_{69}$) (the subscripts refer to the mean degrees of polymerization), in which the corona-forming block is a random brush copolymer of hydrophobic tetradecyl methacrylate (TDMA) and hydrophilic oligo(ethylene glycol) methyl ether methacrylate (OEGMA). Thus, the corona is amphiphilic. This BCP generates a remarkable series of different structures when subjected to crystallization-driven self-assembly (CDSA) in solvents of different polarity. Long ribbon-like micelles formed in isopropanol, and their lengths could be controlled using both self-seeding and seeded growth protocols. In hexanol, the BCP formed more complex structures. These objects consisted of oval platelets connected to long fiber-like micelles that were uniform in width but polydisperse in length. In octane, relatively uniform rectangular platelets formed. Finally, a distinct morphology formed in a mixture of octane/hexanol, namely uniform oval structures, whose height corresponded to the fully extended PFS block. Both long and short axes of these ovals increased with the initial annealing temperature and with the BCP concentration. The self-seeding protocol also afforded uniform two-dimensional structures. Seeded growth experiments, in which a solution of the BCP in THF was added to a colloidal solution of the oval micelles led to a linear increase in area while maintaining the aspect ratio of the ovals. These experiments demonstrate the powerful effect of the amphiphilic corona chains on the CDSA of a core crystalline BCP in solvents of different hydrophilicity.

Received 10th March 2020
Accepted 6th April 2020

DOI: 10.1039/d0sc01453b

rsc.li/chemical-science

Introduction

Block copolymers (BCPs) with a crystallizable block can self-assemble in selective solvents to form micelle-like objects with a semicrystalline core.[1] At temperatures below the melting point of the core-forming polymer, crystallization can provide the driving force for the assembly. This crystallization-driven self-assembly (CDSA) process leads to different types of colloidally stable structures. The earliest examples of CDSA, with poly(ethylene oxide) (PEO) as the core-forming block, led to square platelet structures.[2–5] Later examples, with polyferrocenyldimethylsilane (PFS) as the core-forming block led to rod-like one-dimensional (1D) structures,[6,7] although subsequent examples with shorter corona-forming chains generated more ribbon-like planar (2D) structures, with the core characterized as a single crystal.[8,9] Core-crystalline micelles formed by CDSA have now been reported for BCPs with a broad variety of different core-forming blocks. Examples include poly(3-hexylthiophene),[10] poly(L-lactide),[11–13] polycaprolactone (PCL),[14,15] polycarbonate,[16,17] polyethylene (PE),[5,18–20] oligo(*p*-phenylenevinylene),[21,22] and BCPs with a liquid crystalline block.[23]

The finding of both 1D and 2D objects is consistent with the theoretical predictions of Vilgis and Halperin.[24] In their description, the greatest free energy contribution to self-assembly is the formation of a lamellar crystalline core. The number of folds in the core is determined by a balance of energies that include repulsion between solvent-swollen corona chains. They pointed out that corona repulsion in systems with very long corona chains could limit the extent of lateral growth of the semicrystalline core. This would lead to square micelles if the core chains crystallized at equal rates in both planar directions and elongated micelles if the crystal growth was much faster along one of the crystal growth axes. While the core

[a]*Department of Chemistry, University of Toronto, Toronto, Ontario M5S 3H6, Canada. E-mail: mwinnik@chem.utoronto.ca*

[b]*Department of Chemistry, University of Victoria, Victoria, British Columbia V8W 3V6, Canada*

[c]*Department of Chemical Engineering and Applied Chemistry, University of Toronto, Toronto, ON M5S 3E2, Canada*

† Electronic supplementary information (ESI) available. See DOI: 10.1039/d0sc01453b

of these elongated micelles was predicted to have a rectangular cross-section, the overall shape of micelles that includes the solvent-swollen corona can be thought of as cylindrical, if the core cross section is sufficiently narrow.

From this perspective, for a series of BCPs with a crystalline core-forming block of a given length, the length and dimensions of the corona-forming block should play an important role in determining the morphology formed by self-assembly. Most BCPs examined for their CDSA behavior consist of a crystallizable core-forming block coupled to a soluble corona-forming block. The corona dimensions can be manipulated by varying the length of the soluble block. Some control over the corona dimensions is possible by examining self-assembly of a single BCP in different solvents, but this range is often limited. Generally, solvents employed for self-assembly should be poor solvents for the core-forming block and effective or good solvents for the corona-forming block. Typically, one studies the self-assembly in non-polar solvents of BCPs with a non-polar corona-forming chains such as polydimethylsiloxane (PDMS),[25,26] polystyrene (PS)[2–5,27] or polyisoprene,[9,26,28–30] and in polar solvents for BCPs with a polar corona-forming chain such as poly(acrylic acid),[31–33] or PEO,[17,34–38] or polyvinylpyridine (P2VP),[39–45] or poly(*N*-isopropyl acrylamide).[46–49] Some authors have looked at two-component solvent mixtures, for example tetrahydrofuran/isopropanol (THF/iPrOH) to enhance the solubility of the core-forming block to promote self-assembly,[50] or hexane–iPrOH mixture to create a solvent in which micelles with both PDMS and P2VP corona chains are colloidally stable.[30]

There are very few reports in the literature about how a change in solvent or solvency can affect the morphology of a core-crystalline BCP micelle. Schmalz and coworkers[19] showed that solvent had a strong effect on the self-assembly of PS-*b*-PE-*b*-PMMA (PMMA = poly(methyl methacrylate)) and PS-*b*-PE-*b*-PS when hot solutions of the polymers were cooled. In relatively poor solvents, phase separation occurred above the melting point of the PE block. Spherical micelles formed, and the PE block crystallized upon cooling within the confined geometry of the spherical core. In better solvents, micelle formation occurred at lower temperatures, leading to crystallization-driven formation of elongated micelles. Several papers from Xu and coworkers[51–53] have shown that solvents that promote swelling of the corona chains can induce a morphology change from cylinders to spheres. In another paper,[54] this group showed that addition of hexanol to an aqueous dispersion of spindle-like platelet micelles with a PCL core led to disassembly into elongated micelles. Solvent will also affect the rate of crystallization of the core-forming block. For example, we have shown more rapid micelle growth of PFS-*b*-PDMS micelles in poor solvents for the PFS block like hexane compared to a somewhat better solvent such as ethyl acetate.[55]

In principle, a broader range of solvents can be examined if the corona-forming chains consist of an amphiphilic copolymer. Here we examine the self-assembly of a PFS BCP in which the corona chain is a random copolymer of tetradecyl methacrylate (TDMA) and oligo(ethylene glycol) methyl ether methacrylate (OEGMA, $M_n \approx 300$). We show that the reactivity ratios of both monomers are close to 1. TDMA was chosen because the polymer has a melting point below room temperature,[56] and in this way we avoid complications of corona chain crystallization. The length of the OEGMA was chosen to be similar to that of TDMA pendant group. The homopolymer PTDMA is strongly hydrophobic, readily soluble in hexane and other simple alkanes and insoluble in methanol and ethanol. POEGMA is hydrophilic. It is soluble in water as well as in simple alcohols. This imparts unusual solubility characteristics to the *ca.* 1 : 1 copolymer, which in turn affects the self-assembly of the BCP sample examined here. We examined self-assembly in iPrOH, hexanol and octane, all poor solvents for the core-forming block PFS. We found that this PFS BCP formed ribbon-like micelles in iPrOH, an unusual mixture of structures in hexanol, uniform rectangular platelets in octane, and uniform oval-shaped platelet micelles in a 1 : 1 (v/v) mixture of octane/hexanol. We explore strategies to control the length of the uniform rod-like micelles and the size of the platelet micelles. It is very interesting that such different shapes can be obtained by CDSA of a single BCP through a simple variation of the solvent medium.

Results and discussion

Polymer synthesis and characterization

A random copolymer of tetradecyl methacrylate and oligoethylene glycol methacrylate was synthesized by atom transfer radical polymerization (ATRP) in toluene using 2-azidoethyl 2-bromoisobutyrate as the initiator as described in (ESI†). The reaction was carried out to a monomer conversion of 65% (^{1}H NMR), and the polymer had a composition with a mole ratio of TDMA/OEGMA of 1 : 1.06 (see Fig. S1†). By size exclusion chromatography (SEC) we determined $M_n^{SEC} = 42.7$ kD, $Đ = 1.27$ (see Fig. S2a†). Studies of monomer and polymer composition as a function of conversion for different monomer mixtures showed that these two monomers exhibited similar reactivity ratios ($r^{TDMA} = 0.99 \pm 0.10$, $r^{OEGMA} = 0.98 \pm 0.12$; ESI and Fig. S2b and c†). We conclude that the hydrophobic and hydrophilic pendant groups were randomly distributed along the polymer backbone. Because of the amphiphilic nature of the copolymer, it was not possible to completely remove unreacted monomer by selective precipitation of the polymer in methanol or hexane. This mixture was carried forward into the next step of the synthesis. Because of overlapping peaks in the ^{1}H NMR spectrum, it was not possible to resolve the end groups. The degree of polymerization (DP_n) was characterized after coupling to the PFS block.

The azido-end-capped copolymer was coupled to PFS_{27}-C≡CH by Cu(I) catalyzed azide–alkyne coupling. The synthesis and characterization of PFS_{27}-C≡CH ($DP_n^{MALDI} = 27$, $Đ^{GPC} = 1.05$) has been described previously, and the coupling reaction followed the protocol of our previous publications.[57] The reaction is depicted in Scheme 1. The purification of the BCP to remove homo- and copolymer impurities is described in ESI† and corresponding SEC traces are presented in Fig. S3.† The ^{1}H NMR spectrum of the purified BCP is presented in Fig. S4.† Since the PFS block has a narrow size distribution ($Đ = 1.03$) and has been characterized by MALDI-TOF measurements, it serves as an excellent NMR reference for characterizing the corona-forming

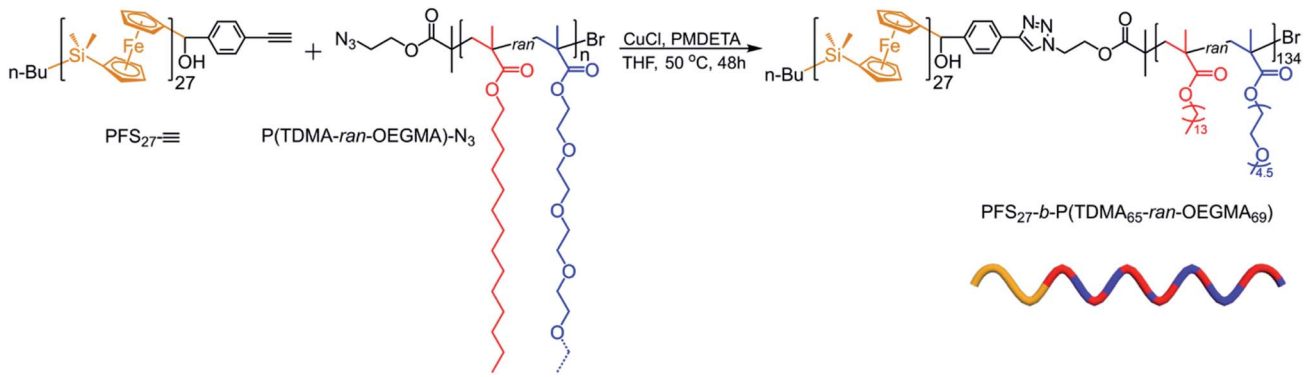

Scheme 1 Synthesis of PFS_{27}-*b*-P($TDMA_{65}$-*ran*-$OEGMA_{69}$) by Cu(I) catalyzed click coupling. The composition of the copolymer block was determined by ^1H NMR by reference to the signals from the PFS_{27} block.

block. In this way we determined that the corona block had an overall $DP_n = 134$ with 65 TDMA units and 69 OEGMA units, *i.e.*, PFS_{27}-*b*-P($TDMA_{65}$-*ran*-$OEGMA_{69}$) ($Đ = 1.17$).

In parallel, we synthesized individual samples of PTDMA and POEGMA homopolymers (for details, see ESI†). These serve as reference points for exploring the solubility of the components of the 1 : 1 random copolymer.

Solubility and cloud point behavior of PTDMA, POEGMA, and P($TDMA_{65}$-*ran*-$OEGMA_{69}$)

To begin, we examined the solubility of PTDMA, POEGMA and their copolymer in a series of alkane and alcohol solvents, which exhibit quite distinctive hydrophilicities. PTDMA (at 10 mg mL^{-1}) was very soluble at room temperature (RT, 23 °C) in octane, hexanol, and in a (1 : 1 v/v) octane/hexanol mixture. It was soluble in hot iPrOH but phase separated upon cooling. A turbidimetric analysis (Fig. 1a) gave a cloud point of *ca.* 70 °C. POEGMA is insoluble in octane. It is very soluble in water but exhibits upper critical solution temperature (UCST) behavior in alcoholic solvents.[58,59] Our sample at 10 mg mL^{-1} was soluble in iPrOH at temperatures down to 10 °C, implying that the cloud point is below 10 °C. It was soluble in warm hexanol with a sharp cloud point at 26.5 °C and in hot octane/hexanol (1 : 1 v/v) with a transition between 50 and 55 °C (Fig. 1b).

The copolymer P($TDMA_{65}$-*ran*-$OEGMA_{69}$) has nearly an equal number of the two pendant groups, which were designed to be of similar length. It exhibited very different solubility behavior. It was soluble in iPrOH and hexanol temperatures between 10 and 80 °C. At 10 mg mL^{-1}, it became soluble in warm octane/hexanol (1 : 1 v/v) and in octane upon heating above 60 °C (Fig. 1c). This difference in solubility profile is related to the copolymer composition, where the PTDMA could decrease the cloud point of POEGMA in hexanol and enhance its solubility in octane as shown in Fig. 1b and c. It is known that the UCST of POEGMA or POEGMA-containing polymers show a dependence on concentration.[59] For the case of P($TDMA_{65}$-*ran*-$OEGMA_{69}$) in octane, we found that the UCST decreased to *ca* 20 °C at 3 mg mL^{-1} and was undetectable at 1 mg mL^{-1}. The POEGMA end group is also known to have a significant influence on its UCST behavior, where flexible end groups were found to lower the critical temperature while rigid aromatic end groups raised the transition temperature.[59] Within the core-crystalline PFS-based BCP micelles, it is foreseeable that the cloud points of the corona chains in the corresponding media would be increased.

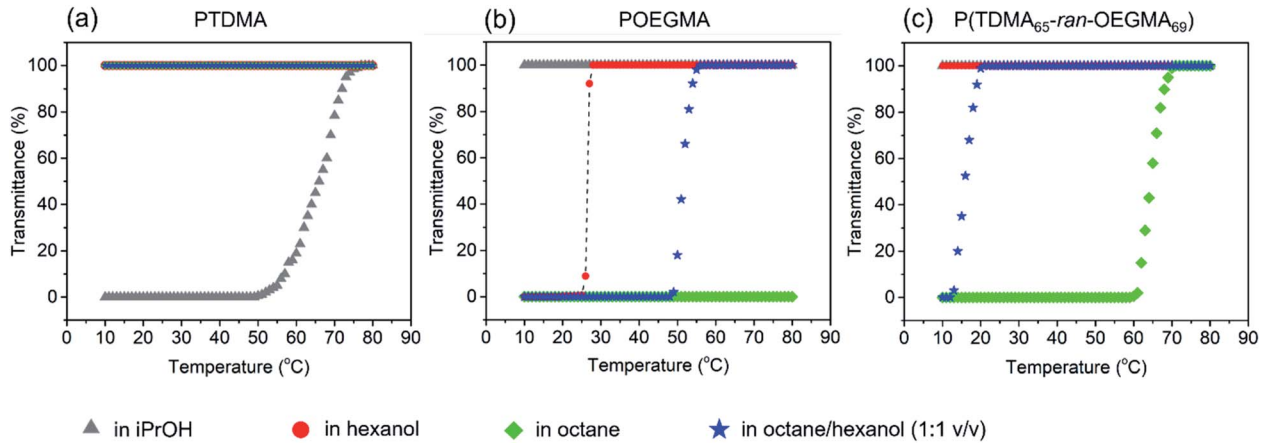

Fig. 1 Turbidimetric analysis of (a) PTDMA, (b) POEGMA, and (c) P($TDMA_{65}$-*ran*-$OEGMA_{69}$) at 10 mg mL^{-1} in four self-assembly media with different hydrophilicity.

These solubility and cloud point measurements serve as a useful guide for defining self-assembly conditions for the PFS_{27}-*b*-P($TDMA_{65}$-*ran*-$OEGMA_{69}$).

Self-assembly in iPrOH

PFS_{27}-*b*-P($TDMA_{65}$-*ran*-$OEGMA_{69}$) was soluble in hot iPrOH (at 0.5 mg mL^{-1}), and upon cooling, long micelles were formed. Transmission electron microscopy (TEM) images (Fig. 2b and S5†) show that the micelles were polydisperse in length but uniform width (W_n = 30 nm, W_w/W_n = 1.03). Corresponding atomic force microscopy (AFM) images (Fig. S6a†) indicate that the micelles have a mean height H_n = 6.5 nm with a narrow height distribution (H_w/H_n = 1.06). In PFS, the Fe–Fe spacing is 0.65 nm (see the XRD spectrum in Fig. S24†),[60,61] from which we

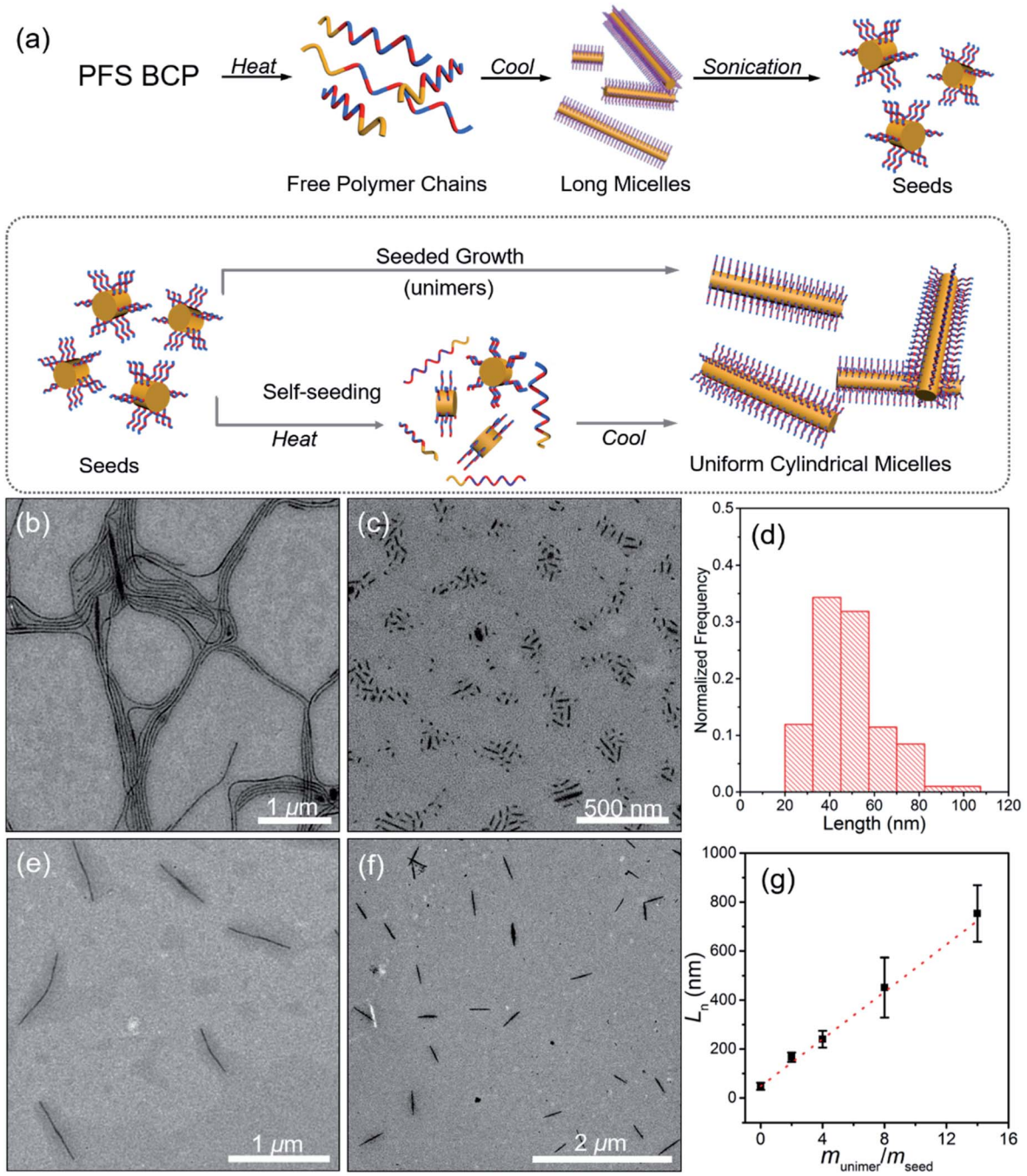

Fig. 2 (a) Schematic representation of self-assembly of PFS_{27}-*b*-P($TDMA_{65}$-*ran*-$OEGMA_{69}$) to form micelles in iPrOH. TEM images of (b) the long micelles and (c) short seeds, and (d) length distribution histogram (L_n = 48 nm, L_w/L_n = 1.09). (e) TEM micrographs of uniform micelles obtained by self-seeding at 70 °C (0.05 mg mL^{-1}. L_n = 661 nm, L_w/L_n = 1.01) and (f) by seeded growth. (g) Plot of L_n *versus* m_{unimer}/m_{seed} for the micelles obtained by seeded growth. The dashed line represents the predicted lengths if all added unimers grew onto the seed micelles. Error bars indicate the standard deviation of the length distribution.

estimate 15 to 19 nm for the length of the fully extended PFS block with $DP_n = 27$, $Đ = 1.05$. If the core height is on the order of 6 nm, we can infer that the PFS block forms two to three folds on average as it packs in the core of these micelles. Since the width determined by TEM is primarily sensitive to the high electron density of the PFS core and is much larger than the height determined by AFM, we infer that these micelles are ribbon shaped and not cylindrical. In fact, close inspection of Fig. 2b shows regions of thicker elongated platelet-like structures, which can be seen more clearly in ESI Fig. S5 and S6c.†

As a general principle, BCPs with a long or highly solvent-swollen corona-forming block tend to form elongated fiber-like micelles, whereas BCPs with shorter, more compact corona chains form platelet-like 2D structures.[8,62] Given the high solubility of the corona-forming block in iPrOH over the entire temperature range of the self-assembly experiments (Fig. 1c), we believed that the swollen corona in iPrOH promoted the formation of the long ribbon-like structures.

We used two approaches in an attempt to generate elongated micelles of controlled length in iPrOH, namely self-seeding and seeded growth. Both approaches start with a sample of the long micelles shown in Fig. 2b. These micelles were subjected to sonication for 30 min at 23 °C. As seen in the TEM image (Fig. 2c), no long micelles survived, and the resulting micelle fragments were characterized by a mean length of $L_n = 48$ nm ($L_w = 52$ nm, $L_w/L_n = 1.09$). These micelle fragments were used as seeds for micelle growth.

Self-seeding. Self-seeding experiments in solution take advantage of the variation in crystallinity of semicrystalline polymer samples. Upon heating, the least crystalline domains dissolve first into unimers. Only the most crystalline domains survive. They serve as nuclei for the epitaxial deposition of unimers as the solution cools.[63] For PFS BCP micelles, we have explained self-seeding in terms of a Gaussian distribution of melting (dissolution) temperatures, and in this way, we can account for the apparent exponential decrease in the number of surviving seed nuclei as the annealing temperature is increased.[64] Fig. 2a provides an overview of the self-seeding mechanism.

Self-seeding experiments were carried out in which samples of PFS_{27}-*b*-P($TDMA_{65}$-*ran*-$OEGMA_{69}$) micelle fragments in iPrOH at 0.05 mg mL^{-1} were annealed for 30 min at temperatures ranging from 60 to 90 °C and then allowed to cool to RT. Fig. 2e shows that the sample annealed at 70 °C upon cooling yielded micelles of uniform length with $L_n = 661$ nm, $L_w/L_n = 1.01$. Fig. S7† shows that the corresponding sample annealed at 80 °C gave micelles characterized by $L_n = 1208$ nm, $L_w/L_n = 1.01$. A sample heated to 90 °C led to μm-size branched micelles (Fig. S7†) with elongated protrusions. It is interesting to note that this BCP, which dissolved initially at 80 °C to yield long micelles, behaved very differently when its micelle fragments were heated to 80 or 90 °C. This difference in behavior is likely a consequence of the increase in crystallinity of the PFS block as the micelle fragments were annealed.

Seeded growth. In a seeded growth experiment, one adds a small volume of a concentrated solution of BCP unimer in a good solvent to a dilute suspension of core-crystalline micelle fragments in a selective solvent. If self-nucleation is slow, then the unimer deposits epitaxially on the open ends of the micelle fragments that serve as seeds for nucleated growth. In this way, one can obtain elongated micelles of uniform length, where the final length obtained is related to the amount of unimer added. For 1D or ribbon-like structures, if the mean number of BCP molecules per unit length does not change, then the final micelle length can be predicted from the ratio of unimer-to-seed.[65]

The short micelle fragments from the sonication step were employed as seeds for seeded growth. The initial seed concentration was 0.05 mg mL^{-1}, and four independent vials with the same volume of seed solution were prepared under the same conditions. Different mass ratios of unimer-to-seed (m_{unimer}/m_{seed}) were obtained by adding different volumes of unimer solution (10 mg mL^{-1} in THF). In this way, micelles with different lengths were prepared (Fig. 2f and S8†). The micelles obtained were uniform in length and similar in width to the starting seeds. For example, with $m_{unimer}/m_{seed} = 4$, micelles with $L_n = 240$ nm, $L_w/L_n = 1.02$ were obtained (Fig. S8b†). Fig. 2g shows that L_n increased linearly with m_{unimer}/m_{seed}. The agreement between the measured L_n values and the theoretical line shows the behavior expected for living CDSA.

In summary, iPrOH is a good solvent for the corona chains of PFS_{27}-*b*-P($TDMA_{65}$-*ran*-$OEGMA_{69}$) over the entire temperature range of RT to 80 °C. When the BCP is heated in this solvent, it dissolved and formed ribbon-like micelles upon cooling, driven by the crystallization of the PFS block. Micelle fragments were formed upon sonication of the long micelles at RT. These could be transformed into uniform structures both by self-seeding and by seeded growth.

Self-assembly in hexanol

When a sample of BCP in hexanol was prepared at a concentration of 0.5 mg mL^{-1} and heated at 80 °C for 60 min and then agitated for a few minutes, the solution turned clear, indicating that the polymer had fully dissolved. Upon slow cooling, structures very different from those formed in iPrOH were observed (Fig. 3). These objects consist of oval platelets connected to long fiber-like micelles that are very uniform in width ($W_n = 20$ nm, $W_w/W_n = 1.02$). These micelles are polydisperse in length and one can see shorter micelles with lengths below 500 nm as well as micelles longer than 5 μm. The AFM image in Fig. S9† shows that the platelets do not appear to be flat and they are typically twice as thick as the fiber-like micelles. There is an overall cluster-like composition to the structures in the images.

In order to explore this self-assembly process, we repeated this experiment but heated the initial solution to 100 °C for 3 h before allowing the sample to cool slowly. As seen in Fig. 3c and d, oval shaped platelets formed, also attached to a network of very long micelles of uniform width. There are many similarities to the structures seen in Fig. 3c, but the platelets are considerably larger and more uniform in size. The fiber-like connectors are very long. A lower magnification image in Fig. 3c shows that the overall shape is flower-like with a dark central core,

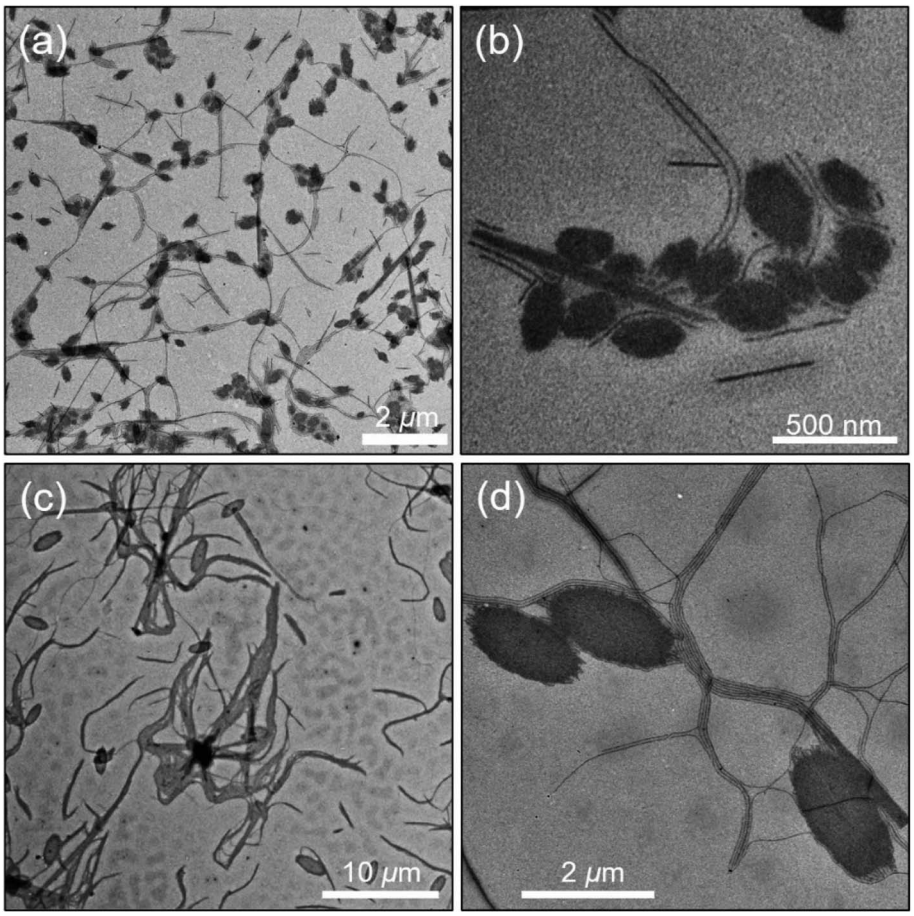

Fig. 3 Low and high magnification TEM images of the structures formed by self-assembly of PFS_{27}-*b*-P($TDMA_{65}$-*ran*-$OEGMA_{69}$) at 0.5 mg mL^{-1} in hexanol (a and b) after heating 60 min at 80 °C and then slow cooling to RT; (c and d) after heating to 100 °C for 3 h before cooling.

with wavy ensembles of fibers that extend tens of μm from the core. Fig. S10a† shows that sonication of the micelles formed at 80 °C leads to a polydisperse mixture of ill-formed structures. Self-seeding experiments with these fragments also afforded mixed morphologies (see ESI and Fig. S10b†).

Hexanol is a less polar solvent than iPrOH. As shown in Fig. 1c, P($TDMA_{65}$-*ran*-$OEGMA_{69}$) is soluble at relatively high concentrations over the entire temperature range examined. Two distinct micelle shapes were obtained, suggesting the corona-forming blocks might promote more than one kind of morphology due to the interaction between them and the solvent.

Self-assembly in octane

The first alkane solvent we examined was decane. A sample of PFS_{27}-*b*-P($TDMA_{65}$-*ran*-$OEGMA_{69}$) at 0.5 mg mL^{-1} dissolved upon heating to 80 °C. Upon cooling, we obtained uniform rectangles with lengths of *ca.* 4 μm and widths of *ca.* 900 nm (TEM images, Fig. S11†). These platelets are fascinating structures and very different from the self-assembled structures obtained in iPrOH or hexanol. In the examples shown in Fig. S11,† one can see that the edges show some local curvature and two of the examples are slightly narrower at one end. The frustrating aspect of this experiment is that after many tries, we were unable to reproduce these simple structures, including by varying the polymer concentration and the annealing temperature. These new experiments led to a precipitate at the bottom of the vial. Thus we turned our attention to octane.

A sample of PFS_{27}-*b*-P($TDMA_{65}$-*ran*-$OEGMA_{69}$) at 0.5 mg mL^{-1} in octane also dissolved when heated to 80 °C for 1 h. Upon slow cooling to RT, we also obtained rectangular platelets as shown in the TEM images in Fig. 4, accompanied by much smaller round spots, which may be due to spherical micelles. The platelets were relatively uniform in size, with a mean long axis of $L_n = 2348$ nm ($L_w/L_n = 1.02$) and a mean width of $W_n = 566$ nm ($W_w/W_n = 1.04$). Each platelet seemly contained a dark circle in the center that spanned the width of the object. We tried to vary the self-assembly conditions to optimize formation of the rectangular platelets. All attempts at varying sample concentration, dissolution temperature or cooling rate for octane as a solvent led to mixed morphologies consisting of platelets and spherical micelles. Nevertheless, we could separate the rectangular platelets from the smaller micelles by selective sedimentation. Using gentle centrifugation (1000 rpm, 10 min, 23 °C), we could selectively sediment a powder that represented the material that formed the dark round spots. The platelets remained in

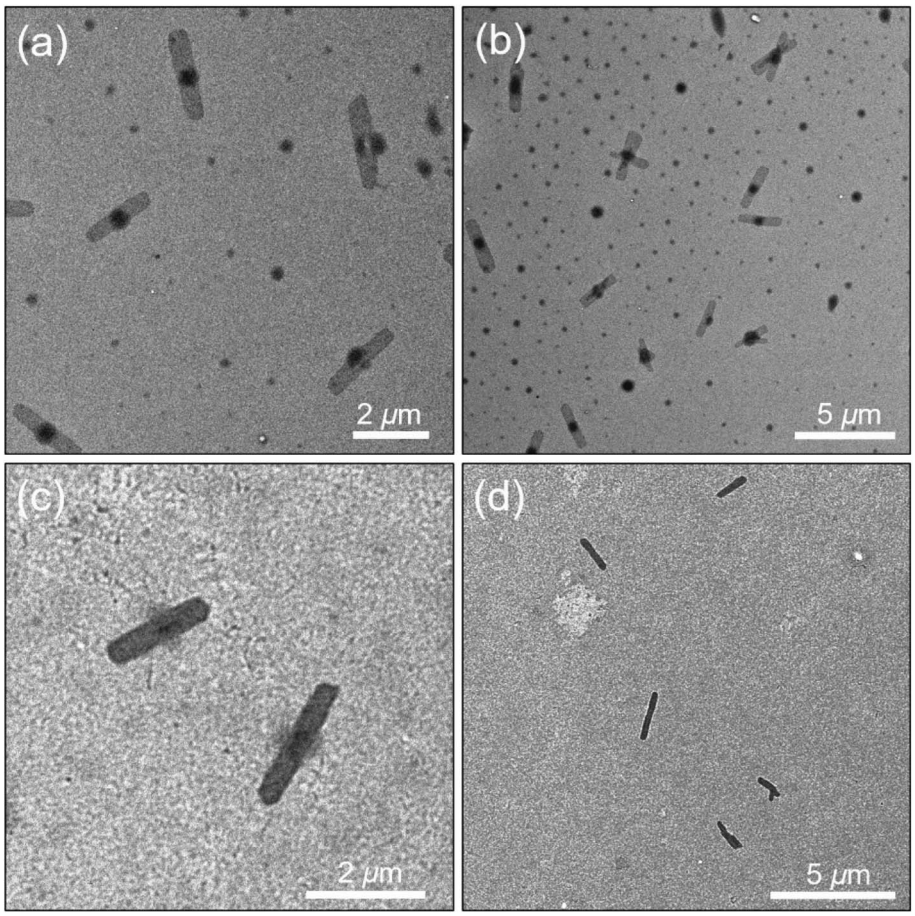

Fig. 4 (a and b) Rectangular platelets obtained by PFS_{27}-*b*-P($TDMA_{65}$-*ran*-$OEGMA_{69}$) in octane. Selective sedimentation removed the material that formed the dark spots (probably due to spherical micelles) in the upper images. (c and d) images of the purified platelets that remained in suspension were collected. (b and d) Lower-magnification images of the structures formed.

suspension. Fig. 4c and d present TEM images of the purified rectangular platelets. An AFM image of one of the separated rectangular platelets (Fig. S12†) shows that it is relatively flat over its entire surface with a mean height of *ca.* 15 nm, which is consistent with extended PFS_{27} chains in the core.

The natural habit of PFS homopolymer crystals is a rectangular platelet, reflecting more rapid growth along the long axis.[66] And PFS BCPs with short corona chains also form rectangular platelet micelles.[9] In the Vilgis and Halperin model, for BCPs with a preferential crystal growth direction, corona repulsion limits crystal growth in the lateral direction. Monte

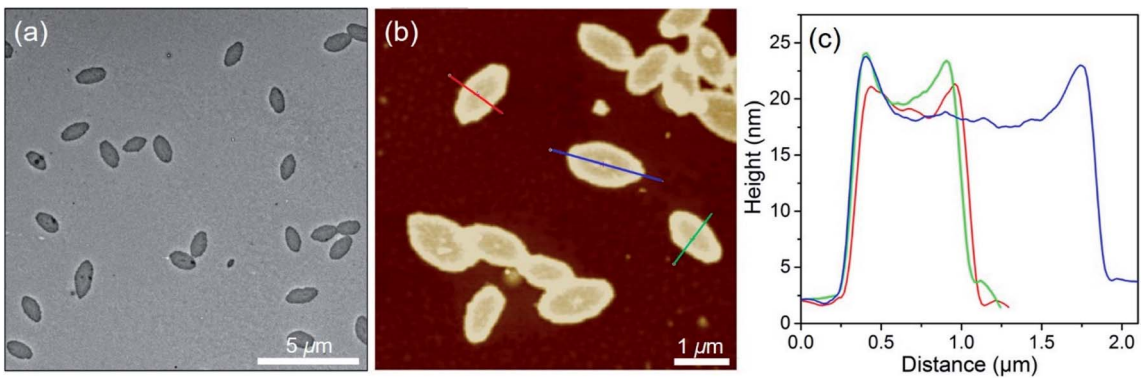

Fig. 5 (a) TEM image of oval micelles by self-assembly in octane/hexanol (1 : 1 (v/v)) (0.5 mg mL^{-1}, 80 °C). (b) AFM image and (c) height profile of oval micelles. The oval long axis $a_n = 1249$ nm, $a_w/a_n = 1.01$. Short axis $b_n = 683$ nm, $b_w/b_n = 1.01$. Area $A_n = 679\,440$ nm^2, $A_w/A_n = 1.02$. Edge height is *ca.* 20 nm and center height is *ca.* 16 nm.

Carlo simulations by Hu and coworkers[67] on crystallization driven fiber growth by BCP predict that growth is retarded in poor solvents for the corona chains. Collapse of the corona chains shields the edges of the growing crystal block, and this effect should also retard 2D growth. From this perspective, the self-assembly of this amphiphilic BCP in octane (and in decane) to give uniform rectangular platelets is unexpected. The platelets themselves are shorter but wider than those formed by PFS BCP examples previously reported,[9] and this likely reflects contributions of the short PFS_{27} block as well as the contracted dimensions of the amphiphilic corona block. The large size for the platelets formed in octane suggests that nucleation is a relatively rare event, whereas the uniform size suggests that nucleation occurs more rapidly than growth. Hot octane and hot decane are much better solvents for PFS than hot iPrOH. This increased solvency likely plays an important role in enabling the PFS chains to assemble onto the edges of the platelets in a more extended conformation.

Self-assembly in a mixed solvent of octane/hexanol

Since hexanol and octane gave such different self-assembled structures under similar protocols, we decided to examine self-assembly in a 1 : 1 (v/v) mixture of octane/hexanol. These results were very different but fascinating.

PFS_{27}-*b*-P($TDMA_{65}$-*ran*-$OEGMA_{69}$) dissolved when heated in the octane/hexanol solvent mixture, and upon cooling, led to the formation of rather uniform planar oval structures, as seen in the TEM image in Fig. 5a. Analysis of multiple micelles with ImageJ determined by measuring more than 200 samples in several images showed that not only the areas had low dispersity (A_n = 679 440 nm^2, A_w/A_n = 1.02) but the long axes (a_n = 1249 nm, a_w/a_n = 1.01) and short axes (b_n = 683 nm, b_w/b_n = 1.01) were also uniform. The aspect ratios were also uniform, with $a_n/b_n = 1.85 \pm 0.06$. An AFM image of the ovals is presented in Fig. 5b. The height profile in Fig. 5c shows an overall concave shape with an edge height of *ca.* 20 nm, and the center is somewhat thinner (16 nm). Multiple ovals are shown in the AFM images in Fig. S13.† These images emphasize the uniformity of the ovals and confirm the observation that the edges are somewhat thicker than the interior. The thickness in the centers of the ovals is more than twice that of the ribbon-like structures formed in iPrOH (*c.f.*, Fig. 2) and is comparable to the mean fully extended length of the PFS_{27} block (17.5 nm).

The formation of uniform oval platelets by PFS_{27}-*b*-P($TDMA_{65}$-*ran*-$OEGMA_{69}$) in a 1 : 1 (v/v) octane/hexanol mixture is unexpected. We have previously reported that PFS BCPs will form pointed oval micelles of uniform size, but only *via* a carefully designed seeded growth protocol[68,69] or addition of substantial amounts of PFS homopolymer.[70] The structures observed here did not require a blend with a large content of PFS homopolymer, nor did it need an intentionally added rod-like seed micelle to catalyze or initiate platelet formation. Because the observation of uniform oval micelles was unprecedented, we designed a variety of new experiments, described below, to explore the scope of this self-assembly process.

Varying the size of the oval micelles

Effect of micelle preparation temperature. In this section, we examine the influence of sample preparation temperature on self-assembly. Aliquots of PFS_{27}-*b*-P($TDMA_{65}$-*ran*-$OEGMA_{69}$) were added to 1 : 1 (v/v) octane/hexanol at 0.5 mg mL^{-1} and heated to different temperatures for 60 min, cooled slowly to RT and then aged 24 h. For sample annealed at 60 °C, the micelles had an overall oval shape but showed fuzzy irregularities at the edges (Fig. S14†). Annealing at higher temperatures (65, 70, 75, 80 °C) led to micelles that were more regular in shape and the edges became better defined (Fig. 5 and S14†). For this range of temperatures, both the long axes and the short axes increased in length with the increase in preparation temperature as shown in Fig. 6a.

Samples prepared by heating the BCP-solvent mixture to higher temperatures (85, 90 °C) gave more complicated structures. As shown in Fig. S15,† the oval structures that formed were filled with dark occlusions that sometimes protruded through the exterior edges. For ovals prepared at 85 °C, we calculate a_n = 3000 nm, a_w/a_n = 1.01 for the long axis and b_n = 1500 nm, b_w/b_n = 1.01 for the short axis. For ovals prepared at 90 °C, the structures were larger, with a_n = 6200 nm, a_w/a_n = 1.003 for the long axis and b_n = 3100 nm, b_w/b_n = 1.004 for the short axis. An AFM image (Fig. S16†) of several ovals in the 85 °C

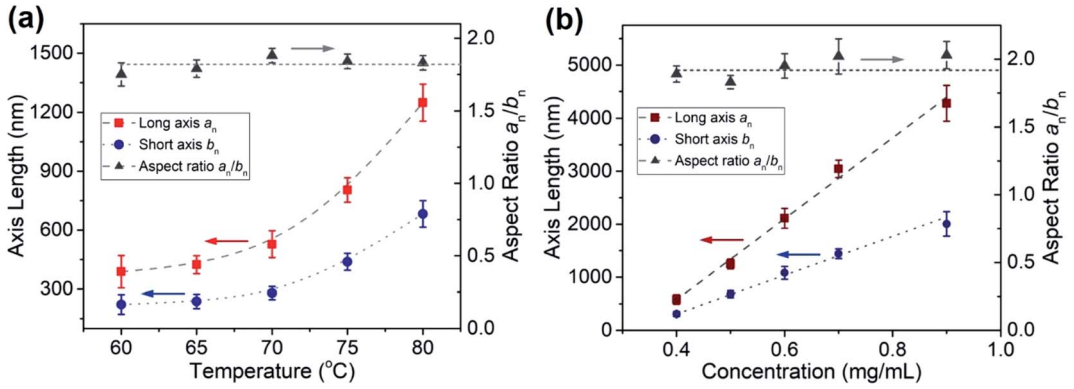

Fig. 6 Effect of (a) sample preparation temperature and (b) initial concentration for micelle preparation at 80 °C on the dimensions of oval micelles formed by PFS_{27}-*b*-P($TDMA_{65}$-*ran*-$OEGMA_{69}$) in 1 : 1 octane hexanol. Values of the corresponding areas are plotted in Fig. S19.†

sample show that the flat portions of the structure are similar in height (20 nm) to those obtained at 80 °C, but the occlusions protrude as high as 60 to 70 nm.

Effect of BCP concentration on micelle formation. We also noted that the concentration of PFS_{27}-*b*-P($TDMA_{65}$-*ran*-$OEGMA_{69}$), ranging from 0.1 mg mL^{-1} to 1.2 mg mL^{-1} affected the size and shape of the micelles formed under the self-assembly conditions described above (1 : 1 v/v octane/hexanol, 80 °C, 1 h, slow cooling, 24 h aging). TEM images of the resulting micelles are shown in Fig. S17.† At 0.1 mg mL^{-1}, dark circles and a few oval structures were observed. At 0.2 and 0.3 mg mL^{-1} oval structures *ca.* 5 μm long and filled with occlusions can be seen. At higher concentrations, the structures were smaller. They were somewhat irregular at 0.4 mg mL^{-1} and became larger and more regular as the sample concentration was increased (Fig. S17†). In Fig. 6b we show that the lengths of both the long axis and the short axis increased linearly as the initial sample concentrations was increased from 0.4 to 0.9 mg mL^{-1}. At the highest concentrations (1.0, 1.2 mg mL^{-1}) the structures became more irregular (Fig. S17†) with occlusions and with a background of dark spots similar to those seen in Fig. 4b above as well as short fiber-like micelles (Fig. S18†).

It is interesting to note that by combining the variables of sample preparation temperature and initial BCP concentration, we can exercise considerable control over the size of the oval micelles obtained. We are able to vary the long axis of these ovals from 390 nm to 4280 nm and the overall area from 65 000 nm^2 to 6 500 000 nm^2 in a well-controlled manner. Plots showing the increases in area with self-assembly temperature and with sample concentration are presented in Fig. S19.†

Self-seeding. We carried out self-seeding experiments in octane/hexanol beginning with a sample of the oval micelles shown in Fig. 5. A sample of these micelles was subjected to bath sonication as described above for ribbon-like micelles in iPrOH. This led to the polydisperse mixture of fragments shown in the TEM images (Fig. S20†). When examined at higher magnification one can see that the larger objects appear to be aggregates of smaller fragments <50 nm in length. The size distribution of the fragments could not be determined.

Self-seeding experiments were carried out at a 10-fold lower concentration than the original oval micelle preparation at 80 °C. Aliquots (1 mL) of these fragments at 0.05 mg mL^{-1} were then annealed 30 min at various temperatures (60, 70, 80 °C), cooled directly to RT and allowed to age for 24 h. Somewhat surprisingly this treatment led to the formation of rounded platelets. Self-seeding at 80 °C yielded uniform ovals with a mean long axis of axis $a_n = 1471$ nm, $a_w/a_n = 1.01$, short axis $b_n = 826$ nm, $b_w/b_n = 1.01$, and areas $A_n = 960\,443$ nm^2, $A_w/A_n = 1.03$. One of the unusual features of this process is that direct self-assembly at this low concentration did not generate uniform ovals, whereas the objects obtained here had dimensions not very different from those obtained by direct self-assembly from octane/hexanol at 0.5 mg mL^{-1} when heated to 80 °C. For example, for the sample shown Fig. 5 prepared by direct self-assembly, we found $a_n = 1249$ nm, $b_n = 683$ nm, both with narrow dispersity.

Self-seeding experiments carried out by sample annealing at 60 and 70 °C gave relatively uniform rounded structures (Fig. S21†) that were not as well defined in shape as those seen in Fig. 7a. For the 60 °C sample, the mean long axis length was 450 nm and the mean short axis width was 293 nm (a_n/b_n ~1.54). For the 70 °C sample, the structures were larger, with a mean long axis length of 590 nm and a mean short axis width of 365 nm (a_n/b_n ~1.62). Both aspect ratios were smaller than that formed at 80 °C in Fig. 5 (a_n/b_n ~1.85) and Fig. 7 (a_n/b_n ~1.78).

"Seeded growth" using intact oval micelles as seeds. Seeded growth experiments with the same micelle fragment sample (Fig. S20a†) used for the self-seeding experiments did not give uniform structures (Fig. S22†). More interesting results were obtained using intact oval micelles as seeds. A sample of the oval micelles shown in Fig. 5 were diluted to 0.05 mg mL^{-1} in 1 : 1 (v/v) octane/hexanol and placed in a series of vials. Then different aliquots (5, 10, 15, 25 μL) of unimer solution (10 mg mL^{-1} in THF) were added to each solution of oval micelles and allowed age at room temperature for 7 days. TEM images of these samples are presented in Fig. 8a–d. Values of the long and short axes as well as the area of the oval structures are presented in Table S3.† These ovals obtained by seeded growth show some internal structure in the TEM images in the form of dark spots or circles. At the highest amount of unimer added ($m_{unimer}/m_{seed} = 5$) the oval structures show a fuzzy boundary. The

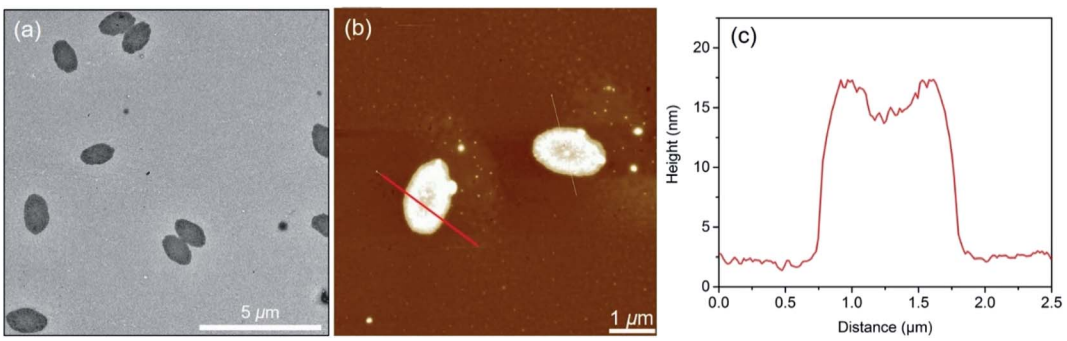

Fig. 7 (a) TEM image of oval micelles by self-seeding of PFS_{27}-*b*-P($TDMA_{65}$-*ran*-$OEGMA_{69}$) seeds (0.05 mg mL^{-1}) at 80 °C in octane/hexanol (1 : 1 (v/v)). (b) AFM image and (c) height profile of oval micelles. The oval long axis $a_n = 1471$ nm, $a_w/a_n = 1.01$. Short axis $b_n = 826$ nm, $b_w/b_n = 1.01$. Area $A_n = 960\,400$ nm^2, $A_w/A_n = 1.03$. The edge height is *ca.* 15 nm and center height is *ca.* 11 nm.

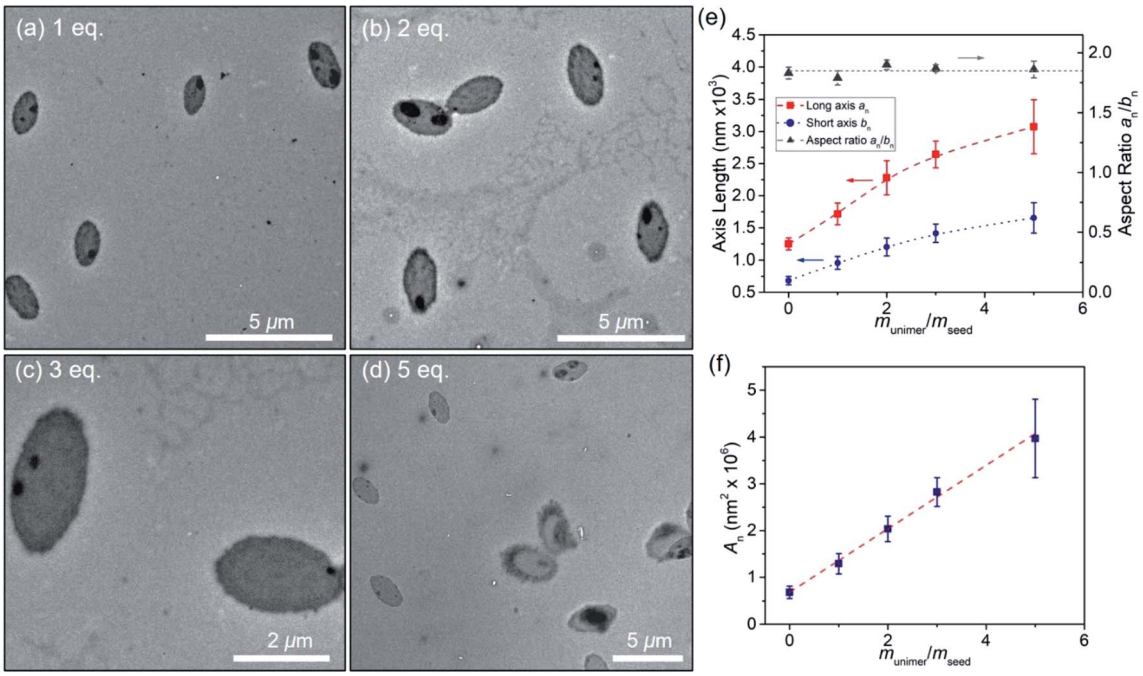

Fig. 8 (a–d) TEM images of oval micelles generated by seeded growth in octane/hexanol (1 : 1 (v/v)) by adding unimers to the oval micelle sample at 0.05 mg mL^{-1} shown in Fig. 5. "eq." refers to the amount of unimer added as m_{unimer}/m_{seed}. (e) Increase in the lengths of the long and short axes of the ovals plotted against m_{unimer}/m_{seed}. (f) Increase in the area of the ovals plotted against m_{unimer}/m_{seed}. The error bars in (e and f) represent the standard deviations in the length or area distribution.

occlusions seen in the TEM images are not apparent in the corresponding AFM images (Fig. S23†), where the most apparent feature is the small difference in height between the edges and the interior of the oval. Fig. 8e shows that the mean values of both the long axis a_n and the short axis b_n increased with the amount of unimer added, but the aspect ratio

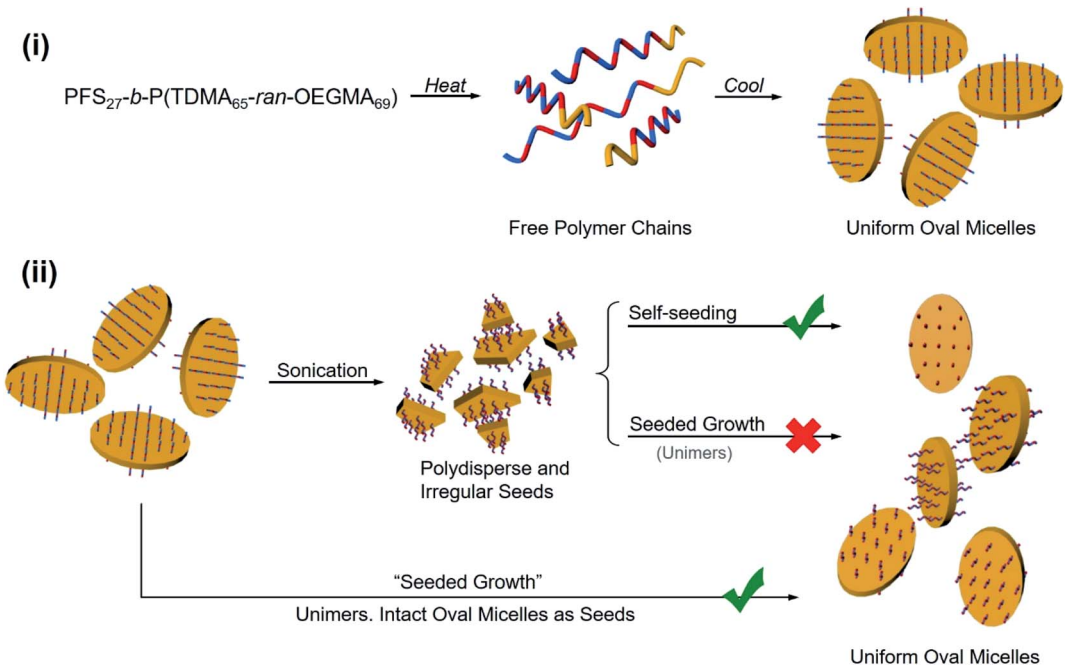

Scheme 2 (i) Schematic representation of the self-assembly of PFS$_{27}$-*b*-P(TDMA$_{65}$-*ran*-OEGMA$_{69}$) to form oval micelles in octane/hexanol (1 : 1 v/v). (ii) Representation of two living CDSA routes for the formation of uniform 2D oval micelles. Upper pathway: micelle fragments generated by sonication generated oval micelles when subjected to the self-seeding protocol. Middle pathway: addition of unimer to the fragments did not lead to uniform structures. Bottom pathway: addition of unimer to a dispersion of intact oval micelles led to seeded growth in which the surface area increased linearly with the amount of unimer added.

remained constant, and the size distribution remained narrow. Fig. 8f reveals that the surface area of these ovals increased in a linear fashion with the ratio m_{unimer}/m_{seed}. This is the expected result if all the unimer grows epitaxially off the perimeter of the ovals and the mean oval thickness does not change.

In Scheme 2 we summarize the processes that led to uniform and regular oval micelles, and the various experiments used to modify the size of the oval micelles generated by PFS_{27}-*b*-P($TDMA_{65}$-*ran*-$OEGMA_{69}$) in 1 : 1 (v/v) octane/hexanol. Uniform oval micelles formed spontaneously when the BCP at 0.5 mg mL^{-1} in the mixed solvent was heated to 80 °C and then slowly cooled to RT. Variation of the BCP concentration and of the annealing temperature prior to cooling led to well-defined changes in the oval size without significant changes in the aspect ratio (*ca.* 1.8) as show in Fig. 6. Sonication of the oval micelles led to irregular fragments. Self-seeding experiments with these micelle fragments regenerated oval micelles, and curiously, these oval micelles reformed at a much lower concentration (0.05 mg mL^{-1}) than was possible in the initial direct self-assembly step. Seeded growth experiments with the micelle fragments failed to give uniform structures. However, seeded growth experiments starting with intact oval micelles led to larger structures that maintained their aspect ratio and with a surface area that increased linearly with the m_{unimer}/m_{oval} ratio.

Conclusions

We report the synthesis of PFS_{27}-*b*-P($TDMA_{65}$-*ran*-$OEGMA_{69}$), a PFS block copolymer with an amphiphilic random copolymer consisting of both hydrophobic $C_{14}H_{29}$ pendant groups and hydrophilic OEG pendant groups of similar length. This polymer undergoes crystallization-driven self-assembly in a variety of different media, ranging in polarity from iPrOH to octane. In iPrOH, it undergoes the "normal" self-assembly expected for a PFS block copolymer with a short PFS block and a much longer corona, forming long narrow micelles of uniform width when a hot solution of the polymer is allowed to cool. These micelles have a ribbon-like shape ($W_n^{TEM} = 30$ nm, $H_n^{AFM} = 6.5$ nm). Upon mild sonication, they form micelle fragments that undergo both self-seeding and seeded growth to form micelles of uniform length and similar width.

In contrast, this BCP forms uniform rectangular platelets with μm dimensions upon cooling hot solutions of the BCP in octane (also decane). Hot solutions of the BCP in hexanol form more complex structures upon cooling. TEM images show both oval platelets and elongated fibers. In a mixed solvent of octane/hexanol (1 : 1 v/v), uniform oval platelet micelles are formed. The height of the micelles is consistent with the fully extended length of the PFS block. The size of the micelles can be varied by changing either the sample dissolution temperature (for a concentration of 0.5 mg mL^{-1}), or for samples heated to 80 °C, by varying the concentration of BCP. When subjected to seeded growth, the area increased linearly with the amount of unimer in THF added. The growth in size preserved the aspect ratio of the ovals ($a_n/b_n = 1.8$).

These variations in morphology are most likely due to changes in solvency of the medium for the corona block. The quality of the solvent for the crystallizable block will, of course, affect the driving force for crystallization and the ease of nucleation of this block in solution. These effects are relatively well explored for PFS BCPs. The effect of solvent on the components of the corona forming chain and on the copolymer itself, as seen in the cloud point plots in Fig. 1, are much more striking. We suspect that hydrogen-bonding contributions from the alcohol-containing media as well as overall solvent polarity play major roles in affecting the dimensions of the corona chains in the micelles.

In summary, the introduction of an amphiphilic corona-forming block into coil-crystalline BCPs represents a new concept for self-assembly that appears to offer substantial flexibility in manipulating the creation and shape of uniform 1D and 2D colloidal structures in solution. Since other types of core-crystalline micelles, for example with a conjugated polymer as the core-forming block, have interesting potential applications as electronic or optical materials, the concept of coil-crystalline BCPs with an amphiphilic corona increases the range of possibilities of the block copolymer toolbox.

Conflicts of interest

The authors declare no competing financial interest.

Acknowledgements

The Toronto authors thank NSERC Canada (grant RGPIN-2017-03741) for their support of this research.

Notes and references

1 W. N. He and J. T. Xu, *Prog. Polym. Sci.*, 2012, **37**, 1350–1400.
2 B. Lotz and A. J. Kovacs, *Kolloid Z. Z. Polym.*, 1966, **209**, 97–114.
3 B. Lotz, A. J. Kovacs, G. A. Bassett and A. Keller, *Kolloid Z. Z. Polym.*, 1966, **209**, 115–128.
4 A. P. Gast, P. K. Vinson and K. A. Cogan-Farinas, *Macromolecules*, 1993, **26**, 1774–1776.
5 E. K. Lin and A. P. Gast, *Macromolecules*, 1996, **29**, 4432–4441.
6 J. Massey, K. N. Power, I. Manners and M. A. Winnik, *J. Am. Chem. Soc.*, 1998, **120**, 9533–9540.
7 J. Raez, R. Barjovanu, J. A. Massey, M. A. Winnik and I. Manner, *Angew. Chem., Int. Ed.*, 2000, **39**, 3862–3865.
8 L. Cao, I. Manners and M. A. Winnik, *Macromolecules*, 2002, **35**, 8258–8260.
9 T. Gädt, N. S. Ieong, G. Cambridge, M. A. Winnik and I. Manners, *Nat. Mater.*, 2009, **8**, 144–150.
10 J. Qian, X. Li, D. J. Lunn, J. Gwyther, Z. M. Hudson, E. Kynaston, P. A. Rupar, M. A. Winnik and I. Manners, *J. Am. Chem. Soc.*, 2014, **136**, 4121–4124.
11 J. X. Zheng, H. Xiong, W. Y. Chen, K. Lee, R. M. Van Horn, R. P. Quirk, B. Lotz, E. L. Thomas, A. C. Shi and S. Z. D. Cheng, *Macromolecules*, 2006, **39**, 641–650.

12 M. Inam, G. Cambridge, A. Pitto-Barry, Z. P. Laker, N. R. Wilson, R. T. Mathers, A. P. Dove and R. K. O'Reilly, *Chem. Sci.*, 2017, **8**, 4223–4230.
13 X. He, Y. He, M. S. Hsiao, R. L. Harniman, S. Pearce, M. A. Winnik and I. Manners, *J. Am. Chem. Soc.*, 2017, **139**, 9221–9228.
14 W. N. He, B. Zhou, J. T. Xu, B. Y. Du and Z. Q. Fan, *Macromolecules*, 2012, **45**, 9768–9778.
15 M. C. Arno, M. Inam, Z. Coe, G. Cambridge, L. J. Macdougall, R. Keogh, A. P. Dove and R. K. O'Reilly, *J. Am. Chem. Soc.*, 2017, **139**, 16980–16985.
16 S. Venkataraman, J. L. Hedrick and Y. Y. Yang, *Polym. Chem.*, 2014, **5**, 2035–2040.
17 J. R. Finnegan, X. He, S. T. Street, J. D. Garcia-Hernandez, D. W. Hayward, R. L. Harniman, R. M. Richardson, G. R. Whittell and I. Manners, *J. Am. Chem. Soc.*, 2018, **140**, 17127–17140.
18 D. Richter, D. Schneiders, M. Monkenbusch, L. Willner, L. J. Fetters, J. S. Huang, M. Lin, K. Mortensen and B. Farago, *Macromolecules*, 1997, **30**, 1053–1068.
19 H. Schmalz, J. Schmelz, M. Drechsler, J. Yuan, A. Walther, K. Schweimer and A. M. Mihut, *Macromolecules*, 2008, **41**, 3235–3242.
20 Q. He, Y. L. Yuan, F. X. Chen, Z. Ma, X. Q. Zhu and R. Song, *Polymer*, 2017, **108**, 322–331.
21 D. Tao, C. Feng, Y. Lu, Y. Cui, X. Yang, I. Manners, M. A. Winnik and X. Huang, *Macromolecules*, 2018, **51**, 2065–2075.
22 L. Han, M. Wang, X. Jia, W. Chen, H. Qian and F. He, *Nat. Commun.*, 2018, **9**, 865.
23 X. Li, Y. Gao, X. Xing and G. Liu, *Macromolecules*, 2013, **46**, 7436–7442.
24 T. Vilgis and A. Halperin, *Macromolecules*, 1991, **24**, 2090–2095.
25 H. Qiu, Y. Gao, C. E. Boott, O. E. Gould, R. L. Harniman, M. J. Miles, S. E. Webb, M. A. Winnik and I. Manners, *Science*, 2016, **352**, 697–701.
26 D. W. Hayward, J. B. Gilroy, P. A. Rupar, L. Chabanne, C. Pizzey, M. A. Winnik, G. A. Whittell and I. Manners, *Macromolecules*, 2015, **48**, 1579–1591.
27 W. Bai, K. G. Yager and C. A. Ross, *Macromolecules*, 2015, **48**, 8574–8584.
28 X. Wang, G. Guerin, H. Wang, Y. Wang, I. Manners and M. A. Winnik, *Science*, 2007, **317**, 644–647.
29 J. S. Qian, G. Guerin, Y. J. Lu, G. Cambridge, I. Manners and M. A. Winnik, *Angew. Chem., Int. Ed.*, 2011, **50**, 1622–1625.
30 P. A. Rupar, L. Chabanne, M. A. Winnik and I. Manners, *Science*, 2012, **337**, 559–562.
31 J. Zhu, S. Zhang, K. Zhang, X. Wang, J. W. Mays, K. L. Wooley and D. J. Pochan, *Nat. Commun.*, 2013, **4**, 2297.
32 D. J. Pochan, J. Zhu, K. Zhang, K. L. Wooley, C. Miesch and T. Emrick, *Soft Matter*, 2011, **7**, 2500–2506.
33 N. Petzetakis, A. P. Dove and R. K. O'Reilly, *Chem. Sci.*, 2011, **2**, 955–960.
34 Z. Deng, S. Yuan, R. X. Xu, H. Liang and S. Liu, *Angew. Chem., Int. Ed.*, 2018, **57**, 8896–8900.
35 A. C. Kamps, M. Fryd and S. J. Park, *ACS Nano*, 2012, **6**, 2844–2852.
36 T. S. Burkoth, T. L. S. Benzinger, V. Urban, D. G. Lynn and S. C. Meredith, *J. Am. Chem. Soc.*, 1999, **121**, 7429–7430.
37 G. Rizis, T. G. M. van de Ven and A. Eisenberg, *ACS Nano*, 2015, **9**, 3627–3640.
38 S. Imai, M. Takenaka, M. Sawamoto and T. Terashima, *J. Am. Chem. Soc.*, 2019, **141**, 511–519.
39 Y. Gao, H. Qiu, H. Zhou, X. Li, R. Harniman, M. A. Winnik and I. Manners, *J. Am. Chem. Soc.*, 2015, **137**, 2203–2206.
40 J. Rao, H. Zhang, S. Gaan and S. Salentinig, *Macromolecules*, 2016, **49**, 5978–5984.
41 R. Vyhnalkova, A. H. Müller and A. Eisenberg, *Langmuir*, 2014, **30**, 5031–5040.
42 J. G. Kennemur, *Macromolecules*, 2019, **52**, 1354–1370.
43 J. Lee, J. Kwak, C. Choi, S. H. Han and J. K. Kim, *Macromolecules*, 2017, **50**, 9373–9379.
44 C. R. Stewart Sloan, R. Wang, M. K. Sing and B. D. Olsen, *J. Polym. Sci., Part B: Polym. Phys.*, 2017, **55**, 1181–1190.
45 M. Ren, Z. Geng, K. Wang, Y. Yang, Z. P. Tan, J. P. Xu, L. B. Zhang, L. X. Zhang and J. T. Zhu, *Langmuir*, 2019, **35**, 3461–3469.
46 D. Tao, C. Feng, Y. Cui, X. Yang, I. Manners, M. A. Winnik and X. Huang, *J. Am. Chem. Soc.*, 2017, **139**, 7136–7139.
47 L. D. Blackman, D. B. Wright, M. P. Robin, M. I. Gibson and R. K. O'Reilly, *ACS Macro Lett.*, 2015, **4**, 1210–1214.
48 J. P. Xu, H. Zhou, Q. Yu, I. Manners and M. A. Winnik, *J. Am. Chem. Soc.*, 2018, **140**, 2619–2628.
49 M. L. Ohnsorg, J. Ting, S. D. Jones, S. Jung, F. S. Bates and T. M. Reineke, *Polym. Chem.*, 2019, **10**, 3469–3479.
50 M. S. Hsiao, S. F. M. Yusoff, M. A. Winnik and I. Manners, *Macromolecules*, 2014, **47**, 2361–2372.
51 W. N. He, J. T. Xu, B. Y. Du, Z. Q. Fan and X. Wang, *Macromol. Chem. Phys.*, 2010, **211**, 1909–1916.
52 W. N. He, J. T. Xu, B. Y. Du, Z. Q. Fan and F. L. Sun, *Macromol. Chem. Phys.*, 2012, **213**, 952–964.
53 J. X. Yang, B. Fan, J. H. Li, J. T. Xu, B. Y. Du and Z. Q. Fan, *Macromolecules*, 2016, **49**, 367–372.
54 X. Y. Wang, R. Y. Wang, B. Fan, J. T. Xu, B. Y. Du and Z. Q. Fan, *Macromolecules*, 2018, **51**, 2138–2144.
55 C. E. Boott, E. M. Leitao, D. W. Hayward, R. F. Laine, P. Mahou, G. Guerin, M. A. Winnik, R. M. Richardson, C. F. Kaminski, G. R. Whittell and I. Manners, *ACS Nano*, 2018, **12**, 8920–8933.
56 K. A. O'Leary and D. R. Paul, *Polymer*, 2006, **47**, 1226–1244.
57 M. Zhang, P. A. Rupar, C. Feng, K. Lin, D. J. Lunn, A. Oliver, A. Nunns, G. R. Whittell, I. Manners and M. A. Winnik, *Macromolecules*, 2013, **46**, 1296–1304.
58 J.-F. Lutz, Ö. Akdemir and A. Hoth, *J. Am. Chem. Soc.*, 2006, **128**, 13046–13047.
59 P. J. Roth, F. D. Jochuma and P. Theato, *Soft Matter*, 2011, **7**, 2484–2492.
60 V. S. Papkov, M. V. Gerasimov, I. I. Dubovik, S. Sharma, V. V. Dementiev and K. H. Pannell, *Macromolecules*, 2000, **33**, 7107–7115.
61 F. Qi, G. Guerin, G. Cambridge, W. Xu, I. Manners and M. A. Winnik, *Macromolecules*, 2011, **44**, 6136–6144.

62 Z. X. Du, J. T. Xu and Z. Q. Fan, *Macromolecules*, 2007, **40**, 7633–7637.
63 J. Xu, Y. Ma, W. Hu, M. Rehahn and G. Reiter, *Nat. Mater.*, 2009, **8**, 348–353.
64 G. Guerin, P. A. Rupar, I. Manners and M. A. Winnik, *Nat. Commun.*, 2018, **9**, 1158.
65 J. B. Gilroy, T. Gädt, G. R. Whittell, L. Chabanne, J. M. Mitchels, R. M. Richardson, M. A. Winnik and I. Manners, *Nat. Chem.*, 2010, **2**, 566–570.
66 G. Cambridge, M. J. Gonzalez-Alvarez, G. Guerin, I. Manners and M. A. Winnik, *Macromolecules*, 2015, **48**, 707–716.
67 J. F. Chen, L. Y. Zha and W. B. Hu, *Polymer*, 2018, **138**, 359–362.
68 A. P. Soto, J. B. Gilroy, M. A. Winnik and I. Manners, *Angew. Chem., Int. Ed.*, 2010, **49**, 8220–8223.
69 Z. M. Hudson, C. E. Boott, M. E. Robinson, P. A. Rupar, M. A. Winnik and I. Manners, *Nat. Chem.*, 2014, **6**, 893–898.
70 A. Nazemi, X. He, L. R. MacFarlane, R. L. Harniman, M. S. Hsiao, M. A. Winnik, C. F. J. Faul and I. Manners, *J. Am. Chem. Soc.*, 2017, **139**, 4409–4417.